JOURNAL OF MATERIALS SCIENCE 27 (1992) 5823–5830

Surface roughness and mechanical properties of melt-spun Al–Cu ribbons

M. A. TAHA, N. A. EL-MAHALLAWY, M. F. ABEDEL-GHAFFAR
Department of Design and Production Engineering, Faculty of Engineering, Ain-Shams University, Cairo, Egypt

Al, Al–5.23, Al–13.46 and Al–33 wt% Cu ribbons with different thicknesses, t, have been prepared by chilled block melt spinning under different processing conditions. Surface roughness, taken as peak to valley values, R_t, measured on both the substrate and air sides of the ribbon, shows great dependence on substrate velocity, v, ejection gas pressure, P, nozzle height above the substrate, H, and a lesser dependence on substrate thermal conductivity, k, and melt superheat, ΔT. The bulk density over all the zones shows an increase over conventionally cast alloys of 7.4% for Al–33 wt% Cu and about 3% for aluminium. Microhardness, H_n, measurements inside each of the three microstructure zones, which were identified across the ribbon section, show variation with t as $H_n = H_0 t^{-m}$, where the constant H_0 depends on the microstructure zone and m depends on the alloy composition. The zone at the substrate side has the highest H_n values and that at the air side has the lowest ones. The number of bending cycles to fracture, which is taken as a measure of ductility, increased with ribbon thickness and decreased with copper content.

1. Introduction

Chilled block melt spinning can be used to produce rapidly solidified ribbons [1–3]. The most common technique for this process is that in which the molten metal stream impinges on the outer rim of a rotating wheel substrate and the centrifugal force acts to throw the ribbon out of the chilled surface. The details of this technique, which was originally developed by Bedall [4] may be found elsewhere [3–7].

Several processing parameters are involved in chilled block melt spinning, mainly the melting crucible, chamber atmosphere, melt superheat, melt ejection nozzle diameter, melt ejection pressure and head, wheel substrate material and surface conditions, as well as the wheel rotation speed [8–14].

The average cooling rates achieved in chilled block melt spinning lie between 10^3 and 10^7 K s^{-1} [9–11, 15–17]. Cooling rates up to 10^5 K s^{-1} result in the production of microcrystalline ribbons and higher rates result in amorphous ribbons. Both microcrystalline and amorphous ribbons, produced by the melt spinning process possess highly improved properties [8–11, 18–27]. If the microcrystalline ribbons are considered, a number of improvements in structure and properties are obtained [13, 18, 28–31]. These include refined grain size (0.5–10 μm) and second-phase particles, changing segregation with an ability to minimize formation of the coarse brittle intermetallic segregation phase [30, 31], increasing solid solubility range and the possibility of the formation of other stable and metastable phases [18, 28].

In general, a remarkable improvement in the properties of alloys prepared by rapid solidification have been reported in the literature. These properties include different physical, electrical, magnetic, thermal and mechanical ones [8–11, 14–17, 28–31].

The application of rapid solidification to aluminium and its alloys, in particular, has been shown to improve formability, ductility, fracture toughness, hardness, fatigue strength, and stress corrosion life, in the case of many commercial aluminiums and aluminium alloys, [11, 18–27]. On the other hand, the ribbon dimensions, i.e. thickness, width and length, have been a subject for experimental studies and modelling [8–17]. However, the surface roughness and topography of the ribbon have only received little attention [11, 14, 32, 33].

The purpose of this paper is to present some experimental results obtained on the surface roughness of both surfaces of the ribbon produced by chilled block melt spinning, as well as results of hardness and ductility measurements. The alloys considered are commercial purity aluminium and Al–Cu alloys with different copper contents. In previous papers, the cooling rate calculations [17], ribbon dimensions [12] and microstructure [13] of the same alloys have been given.

2. Experimental procedure

The chilled block melt spinning technique was used to prepare ribbons of aluminium and Al–Cu alloys with 5.23, 13.46 and 33 wt % Cu, under an inert gas atmosphere. The material used had an impurity content of 0.01% maximum. The wheel substrate diameter was 200 mm. Different processing conditions were used in

0022–2461

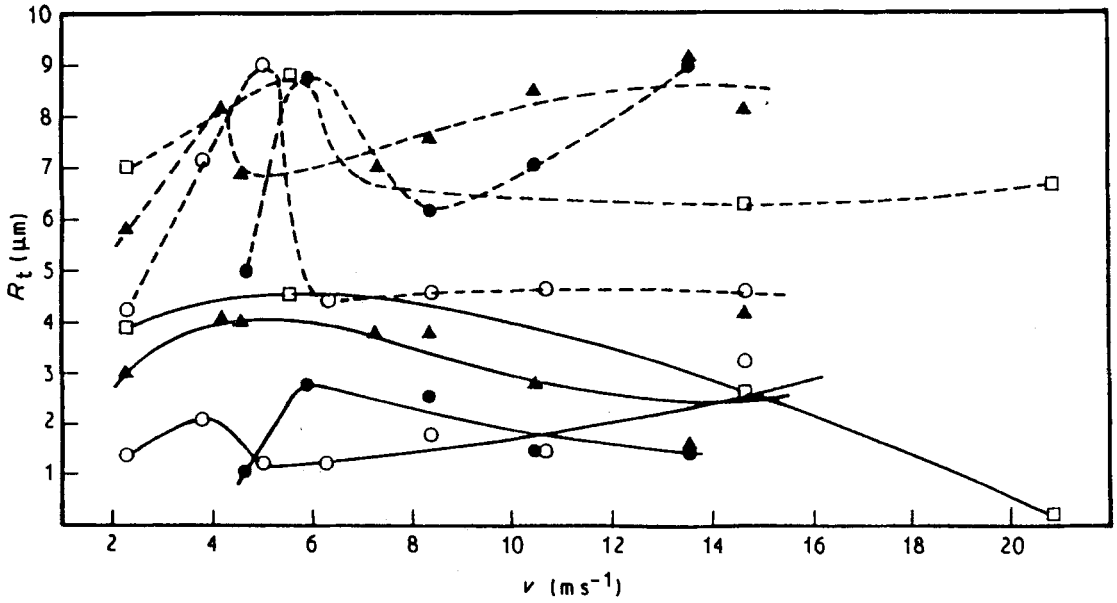

Figure 1 Variation of ribbon surface roughness, R_t, with substrate linear velocity, v: (---) AS surface, (——) SS surface, $P = 2.9 \times 10^4$ N m^{-2}, $\Delta T = 50$ K, $K = 390$ W m°, $H = 7$ mm, $d = 1$ mm. (▲) Pure Al (99.99%), (○) Al–5.23 wt % Cu, (□) Al–13.46 wt % Cu, (●) Al–33 wt % Cu.

order to produce ribbons with different microstructures and external features (thickness, width and length) as well as different surface roughness. These processing conditions include the variation of substrate peripheral velocity, v, from 2–22 m s^{-1}, the substrate thermal conductivity, k, to be 45, 90 and 390 W m^{-2} K^{-1} by using different wheel materials (steel, brass and copper, respectively), the melt pouring superheat, ΔT, from 0–150 K, the gas pressure for the melt ejection at the nozzle orifice, P, from 2.9×10^4–6.8×10^4 Pa, the nozzle height above the substrate, H, from 5–20 mm while the nozzle orifice diameter was kept constant to 1 mm. Care was always taken to clean and then to polish the substrate surface between each experiment in a similar way by using a standard SiC paper of 1000 grid size.

The surface roughness for both substrate (SS) and air (AS) sides of the ribbon was taken as the maximum peak to valley height, R_t. This was measured by using a teleserve apparatus. Measurements were made along ribbon width taking the average of several readings representing different ribbon areas.

3. Results and discussion

3.1. Surface roughness

3.1.1. Influence of v

The variation of the average roughness, R_t, with substrate linear velocity, v, for both substrate side surface (SS) and air side surfaces (AS) is indicated in Fig. 1 for the different Al–Cu alloys studied. It is clear that R_t values for AS are always higher than SS in the same ribbons. At the ribbon AS surface, R_t increases sharply on increasing v up to a value, depending on the alloy composition, ranging between 4 m s^{-1} for pure aluminium and 6 m s^{-1} for Al–33 wt % Cu, where a maximum value of R_t is obtained. On further increasing v, R_t decreases sharply to a minimum value depending on the alloy composition, then increases again slightly, or remains almost constant in some cases.

At the ribbon SS surface, the effect of v on R_t is weaker so that R_t increases slightly to a maximum value at a critical v similar to that for the AS surface. A slight decrease in R_t is then observed beyond the critical v value. Similar measurements have not been found in the literature to allow comparison. However, Miyazawa and Choh [32], who worked on Pb–17 wt % Sb, have defined a theoretical summation for the surface roughness on both SS and AS (R_{ts}) which equals the difference between the measured and the calculated (weight/length × width) ribbon thicknesses. These results are replotted with the present results in Fig. 2. They show a decreasing R_{ts} with v, starting by a

	Alloy composition	d (mm)	P (N m^{-2})	ΔT (K)	H (mm)
1	Al–pure (99.99%)	1	2.94	50	7
2	Al–5.23 wt % Cu	1	2.94	50	7
3	Al–13.46 wt % Cu	1	2.94	50	7
4	Al–33 wt % Cu	1	2.94	50	7
5	Pb–17.5 wt % Sb [32]	0.62	0.39	150	5
6	Pb–17.5 wt % Sb [32]	1.49	0.39	150	5
7	Pb–17.5 wt % Sb [32]	2.04	0.39	150	5

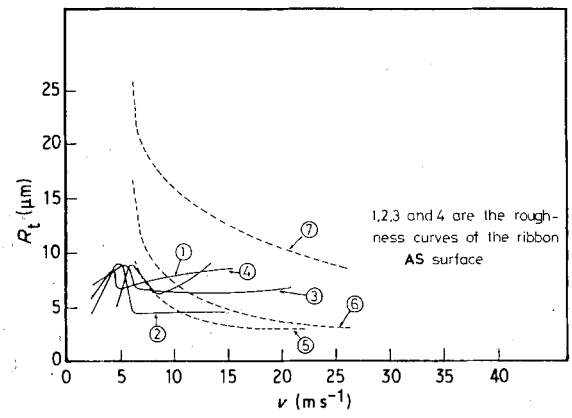

Figure 2 Influence of substrate linear velocity, v, on the summation ribbon surface roughness, R_{ts}, obtained by Miyazawa and Choh [32] compared with R_t from the present work.

sharp decrease at $v = 5$–$6\ m\ s^{-1}$, then the decrease is gradual up to $25\ m\ s^{-1}$ indicating a behaviour similar to the present one when starting with the critical v values. However, the absolute values of R_{ts} of Miyazawa and Choh cannot be taken as a real surface roughness index and they better denote an average deviation from the expected to the measured thicknesses.

3.1.2. Influence of thermal variables, k and T

The influence of the substrate thermal conductivity, k, changed on using different substrate materials (steel, brass and copper) and the influence of melt superheat was examined for the Al–5.23 wt % Cu alloy. The variation of surface roughness, R_t, with k, for both SS and AS surfaces, is not strong, as shown in Fig. 3. On increasing the thermal conductivity, k, R_t only slightly increases up to $k = 100\ W\ m^{-1}\ K^{-1}$, then remains almost constant. The effect of melt superheat, T, is shown in Fig. 4. Behaviour opposite to the influence of k can be seen, where R_t increases with decreasing T to a critical value of 973 K, below which an almost constant R_t is obtained. By using either high superheat or a substrate material with lower k, the impinging melt puddle will have a longer dwell time in which to spread while the surface tension is low, before complete solidification and therefore a better surface with lower R_t is obtained.

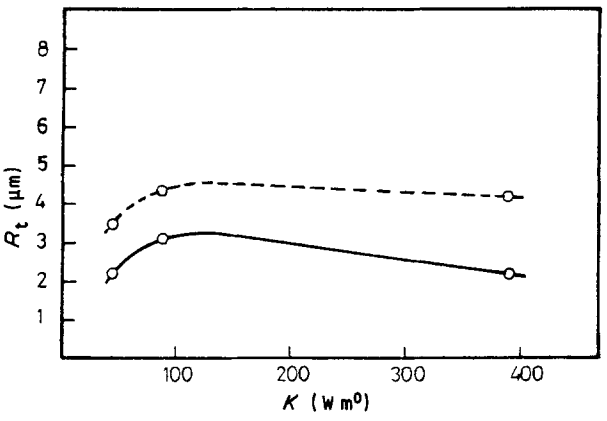

Figure 3 Influence of substrate thermal conductivity, k, on ribbon surface roughness, R_t: (---) AS surface, (——) SS surface, $v = 19\ m\ s^{-1}$, $P = 4.9 \times 10^4\ N\ m^{-2}$, $\Delta T = 50$ K, $H = 7$ mm, $d = 1$ mm. (○) Al–5.23 wt % Cu.

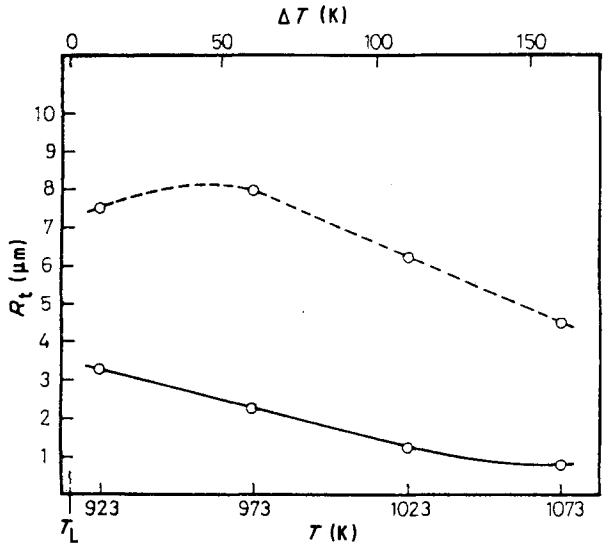

Figure 4 Variation of ribbon surface roughness, R_t, with melt temperature, T, or melt superheat, ΔT. (---) AS surface, (——) SS surface, $v = 15\ m\ s^{-1}$, $P = 2.9 \times 10^4\ N\ m^{-2}$, $K = 390\ W\ m°$, $H = 7$ mm, $d = 1$ mm. (○) Al–5.23 wt % Cu.

3.1.3. Influence of P and H

As shown in Fig. 5, a strong effect of the ejection gas pressure, P, on R_t for both SS and AS surfaces, is observed for Al–2.23 and Al–13.46 wt % Cu ribbons. Generally, R_t increases to a maximum on increasing P to a critical value of 4×10^4 and 5×10^4 Pa for Al–5.23 and Al–13.46 wt % Cu, respectively. Beyond the critical value, R_t decreases.

The theoretical summations of surface roughness, R_{ts}, calculated by Miyazawa and Choh [32] for both SS and AS surfaces for Pb–17 wt % ribbons are replotted together with the present results as shown in Fig. 6. For the range of P from 2×10^4–5×10^4 Pa, which is common in both works, both Al–Cu and Pb–Sb alloys show nearly similar behaviour and the R_t values range between 3 and 8 μm for both alloys.

Fig. 7 shows the variation of R_t with H. For the SS surface. R_t increases to a maximum value of 5 μm on increasing H to a critical value of $H = 12$ mm, after which R_t decreases gradually. For the AS surface, R_t seems to have maximum of 10 μm at $H = 6$ mm, beyond which it decreases gradually.

The effect of P and H on SS surface roughness is similar. First R_t increases with increasing P or H, probably due to the melt impact and rebound occurring on the wheel surface, which increase with the stream velocity. At the same time, increasing P or H improves the wetting pattern [34], hence fewer air pockets are formed. This factor becomes more effective beyond the critical pressure or head and R_t of the SS surface with increasing P or H.

The roughness of the AS surface follows the same behaviour as the SS surface, but with higher values,

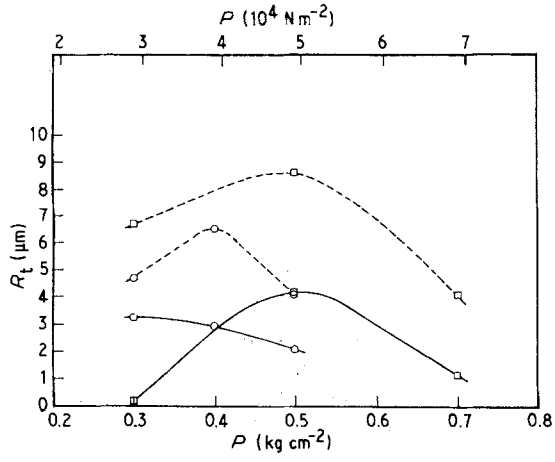

Figure 5 Variation of ribbon surface roughness, R_t, with ejection gas pressure, P. (---) AS surface, (——) SS surface. (○) Al–5.23 wt % Cu, (□) Al–13.46 wt % Cu. $v = 19\ m\ s^{-1}$, $\Delta T = 50$ K, $K = 390\ W\ m°$, $H = 7$ mm, $d = 1$ mm.

	Alloy composition	d (mm)	v ($m\,s^{-1}$)	T (K)	H (mm)
1	Al–5.23 wt % Cu	1	21	50	7
2	Al–13.46 wt % Cu	1	21	50	7
3	Pb–17.5 wt % Sb [32]	1.49	13	150	5
4		1.1	13	150	5
5		0.62	13	150	5

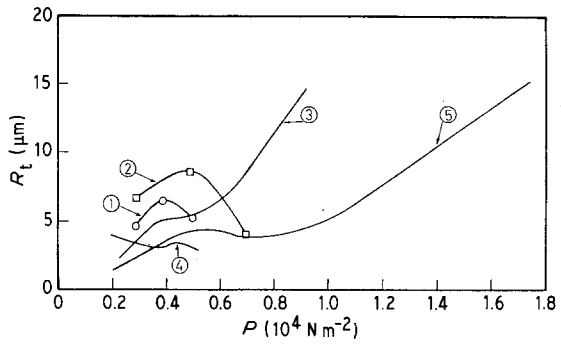

Figure 6 Variation of summation ribbon surface roughness, R_{ts}, with ejection gas pressure, P, obtained by Miyazawa and Choh [32] compared with R_t, that of the present work. Curves 1 and 2 are the roughness curves of the ribbon AS surface.

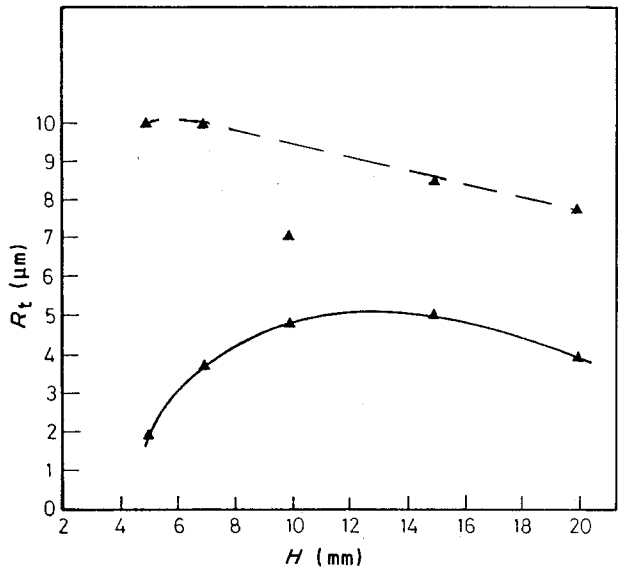

Figure 7 Influence of nozzle–substrate distance, H, on ribbon surface roughness, R_t. (---) AS surface, (——) SS surface. (▲) Pure Al (99.99%), $v = 6.3\ m\,s^{-1}$, $P = 2.9 \times 10^4\ N\,m^{-2}$, $\Delta T = 50$ K, $K = 390$ W m°, $d = 1$ mm.

because the roughness of a solidifying free surface is always more than a surface in contact with a metal substrate.

3.1.4. Microscopic observations of surface roughness

SEM was used for the observations of both SS and AS surfaces at different magnifications in order to examine the surface roughness forms appearing. At the SS, air pockets are observed at × 100. These air pockets exhibit a heterogeneous distribution, as shown in Fig. 8. On increasing the substrate linear velocity, v, both the size and area of the air pockets were reduced, resulting in a better surface roughness at the SS

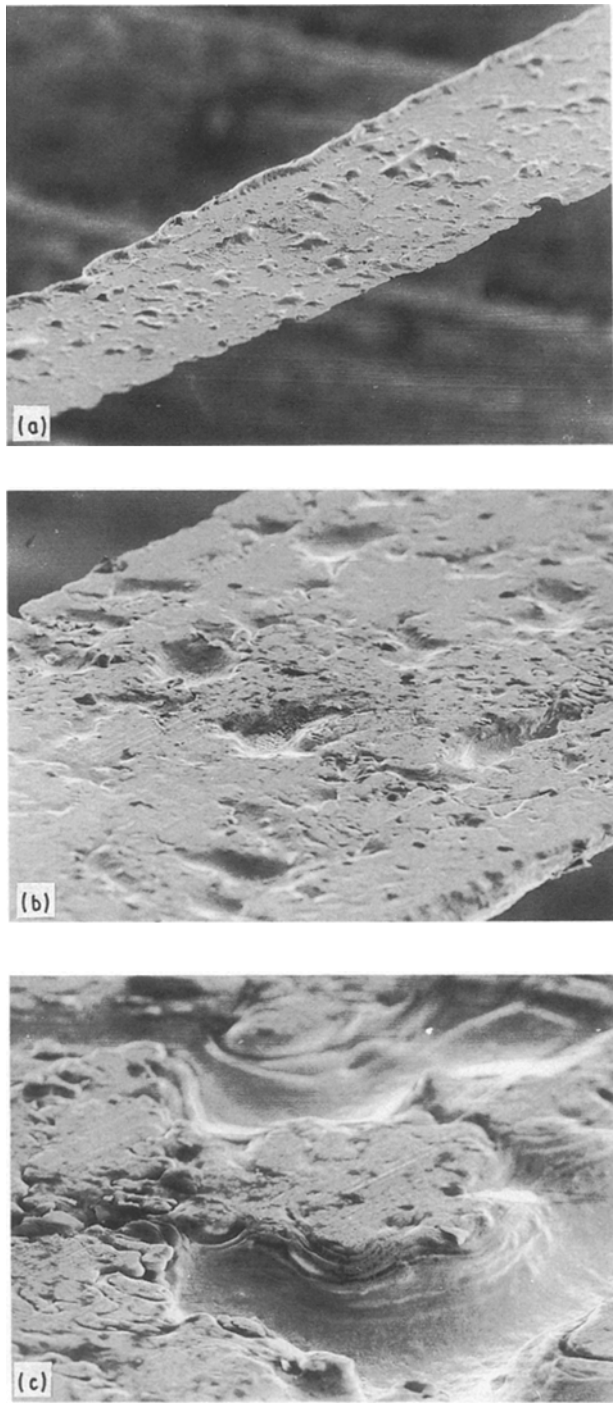

Figure 8 Scanning electron micrographs showing air pockets on the ribbon SS surface. (a) The heterogeneous distribution of the air pockets on ribbon substrate-side surface, × 30. (b) Shape of the air pockets, × 100. (c) Air pockets on ribbon substrate-side surface showing its random shape, × 300.

surface. This is correlated with R_t measurements in Fig. 1, so that the present results seem to be in agreement with Huang and Fiedler [33] who reported that the roughness of the ribbon substrate surface is due to the air pockets which are trapped during the process. They indicated that the air-pocket distribution and size are functions of the substrate material and of the substrate linear velocity. The same authors found that the use of matte substrate wheel surface (i.e. increasing its roughness) and increasing of the wetting characteristic of the alloy on the used substrate surface (mainly the wetting angle), reduce the number of

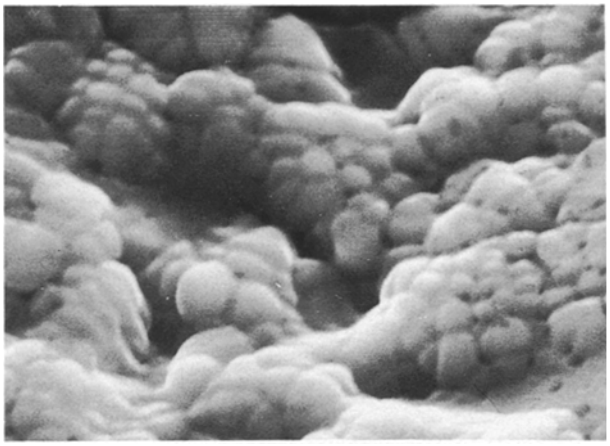

Figure 9 Scanning electron micrograph showing dendrite protrusion inside air pockets at the SS surface. × 3000.

pockets obtained and ensure heterogeneous air-pocket distribution.

Careful SEM examinations at × 3000, Fig. 9, show dendrite protrusion inside the air pockets which can be considered as a secondary surface roughness. Another source of roughness is formed in the case of a copper substrate, where some microscopic pieces of the cast ribbon are found to be stuck on the SS side of the ribbon. This tendency of the aluminium melt to stick to the copper substrate is expected. This defect could be eliminated by using a chromium-coated copper substrate or a copper–1% chromium substrate to reduce the sticking of aluminium on its surface [33].

Microscopic observation of the AS surface of the ribbon at low magnifications up to × 100 reveals the main roughness waves on that surface, Fig. 10, which are wider in the case of ribbons made of pure aluminium. These roughness waves are due to the high surface tension of the aluminium alloys and can be minimized by casting in vacuum or an inert gas atmosphere [35]. Another possibility for minimizing this defect is by modifying the aluminium alloy wetting characteristic through changing its chemical composition [33]. The better surface quality for the Al–13 wt % Cu over the Al–5.7 wt % Cu ribbons observed in this work, is due to this reason.

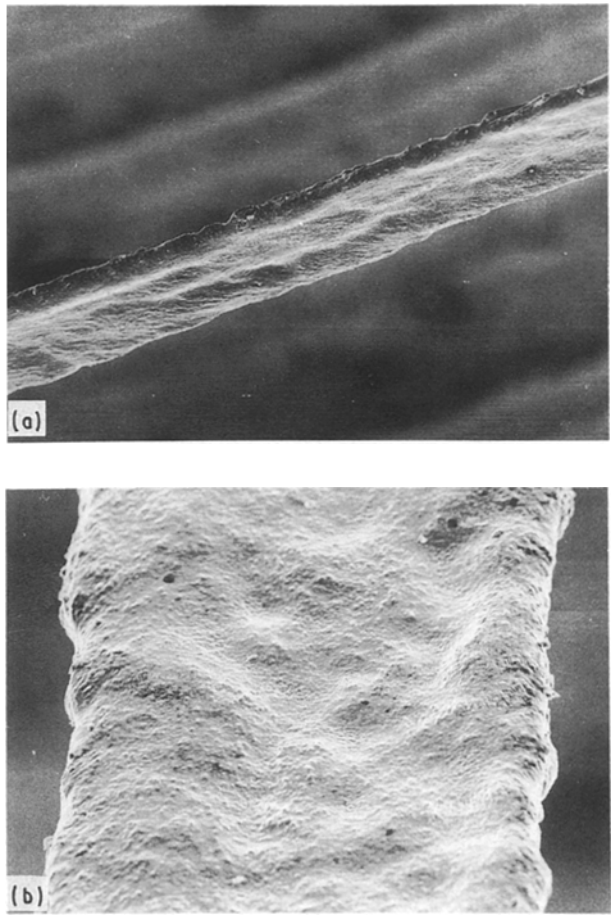

Figure 10 Scanning electron micrographs showing the main surface roughness waves obtained on the ribbon AS surface. (a) × 30, (b) × 70.

3.2. Physical properties

3.2.1. Density

Fig. 11 shows the density values, ρ, of rapidly solidified, melt-spun (RSP) ribbons for different thicknesses, t, as well as the density of conventionally cast (CC) alloys (rods 12 mm diameter cast in a graphite mould). The results indicate that the density of RSP is higher than that of the CC specimens for all alloy compositions under consideration. This increase in density reaches 7.4% for Al–33 wt % Cu and about 3% for pure aluminium.

The improvement in the density of RSP ribbons over CC ones could be as a result of the minimization of porosity and/or the formation of other phases. For the Al, Al–5.23 wt % Cu and Al–13.46 wt % Cu alloys, the RSP densities reach 2.7, 2.8 and 2.92 $kg\,m^{-3}$, respectively, which are similar to the theoretically estimated ones. In this case, the improvement in density is only due to the absence of porosity in the RSP ribbons. In the case of Al–33 wt % Cu alloy, the RSP density reaches 3.72 $kg\,m^{-3}$, in comparison with a theoretically estimated value of 3.46 $kg\,m^{-3}$, indicating an improvement due to both minimized porosity and the presence of other phases. The possible phases formed in these specimens [13], in addition to aluminium and $CuAl_2$ are CuAl, Cu_3Al_2, Cu_9Al_4 and Cu_3Al.

3.3. Mechanical properties

3.3.1. Microhardness

The Vicker's microhardness was measured using a 2 μm pyramid and a load ranging between 2.5 and 250 kgf depending on the alloy composition and ribbon thickness. Fig. 12 shows the microhardness values for each of the three microstructural zones which were identified across the ribbon thickness, as well as the bulk microhardness of the ribbon. The microstructural zones have been described in a previous paper [13]. The hardness of the CC alloys is indicated in the figure for comparison.

Microhardness values generally increase for thin ribbons due to the increase in cooling rate resulting in a finer microstructure. For each alloy a family of

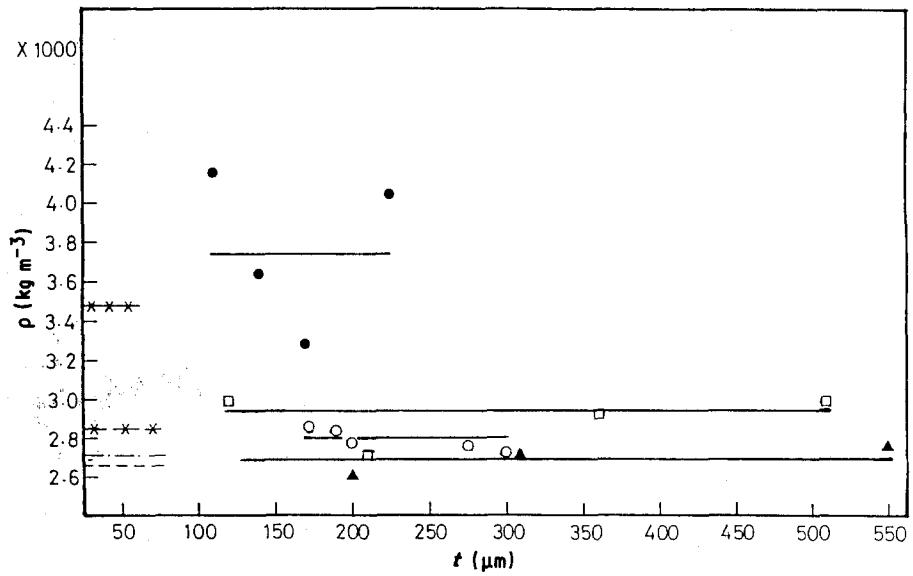

Figure 11 The effect of increasing ribbon average thickness, t, on alloy density, ρ. (▲) Pure Al (99.99%), (○) Al–5.23 wt % Cu, (□) Al–13.46 wt % Cu, (●) Al–33 wt % Cu; nominal densities for the conventionally cast alloys represented, respectively, by (– – –), (— · —), (-X-X-) and (-X—X-).

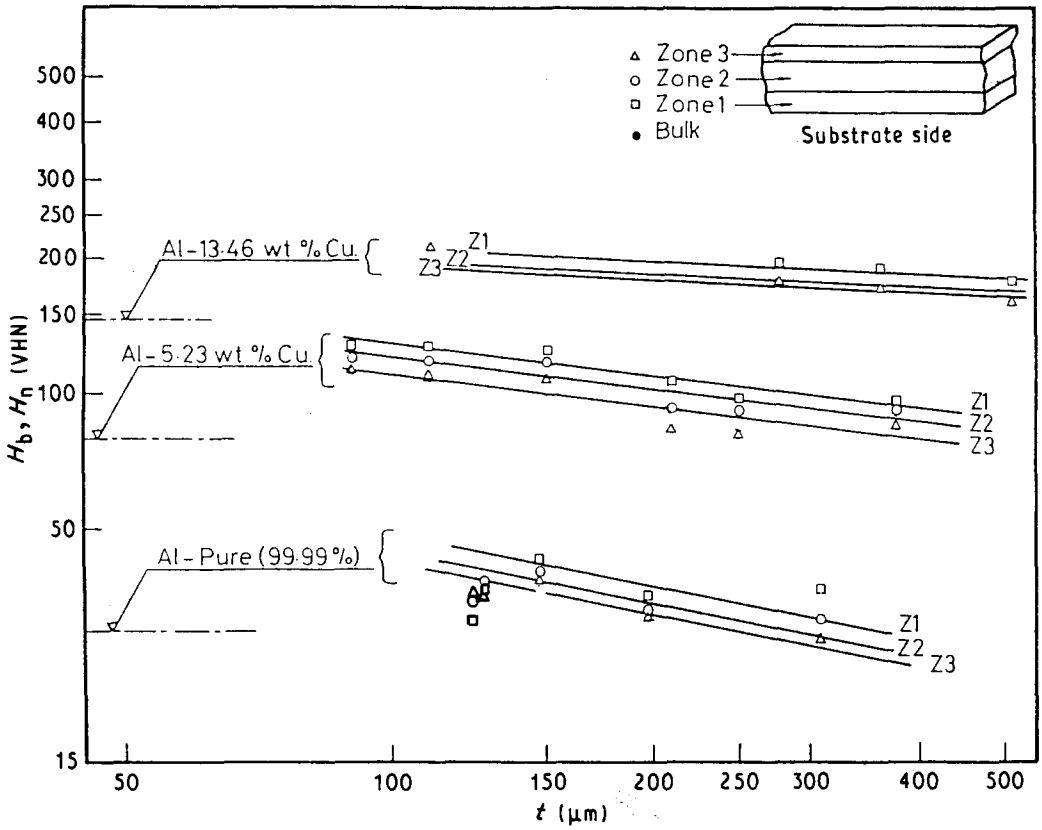

Figure 12 Influence of ribbon average thickness, t, on ribbon microhardness, H, in each microstructural zone. (———) Conventionally cast alloy, measured hardness.

parallel straight lines is obtained following the relationship

$$H_n = H_0 t^{-m} \quad (1)$$

where H_n is the zone microhardness, H_0 is a constant dependent on the zone and the cooling rate in each zone, t is the average ribbon thickness (μm) and m is an exponent depending on the alloy composition (amount and type of precipitates). Table I summarizes the values of H_0 and m for each zone.

A comparison of the hardness of RSP and CC alloys indicates that using RSP, the hardness increased by 51.6% for Al–33 wt % Cu, 22% for Al–13.46 wt % Cu, 21% for Al–5.23 wt % Cu and 12.2% for Al. Katgerman *et al.* [36] have found an increase in hardness of 27% for wrought aluminium alloy by using RSP. In the present results the increase in hardness of pure aluminium is the least compared with other Al–Cu alloys. This is because the change in hardness for aluminium is due to the finer grain size

TABLE I Values of constants H_0 and m, in $H_n = H_0 t^{-m}$ for the different alloys

Alloy composition	Zone	H_0 (VHN)	m
Al, pure (99.99%)	Z1	327.68	− 0.41
	Z2	300.37	
	Z3	280.87	
Al–5.23 wt % Cu	Z1	340.17	− 0.213
	Z2	316.91	
	Z3	293.65	
Al–13.46 wt % Cu	Z1	307.62	− 0.081
	Z2	288.11	
	Z3	277.61	

while in other alloys, it is due to the reduction in size of precipitates mainly $CuAl_2$ hard phase and to the presence of metastable phases in addition to this fineness of microstructural features.

The comparison between the hardness of different microstructure zones indicates that the hardness in zone 1 in contact with the substrate wheel is the highest followed by that of the central one, zone 2, and that on the air side, zone 3. Actually, these zones may be distinguished as three different morphological zones across the ribbon thickness: zone 1, with a fine equiaxed or "featureless" structure; zone 2 with a columnar structure extending up to two-thirds of the ribbon thickness; and zone 3 with coarse equiaxed grains at the air side.

In general, the fine structure in zone 1, has fine copper-rich precipitates. Zone 3 contains larger grains with a lower density of copper-rich precipitates, while zone 2 is intermediate [13]. In ribbon thicknesses up to 90 μm, some metastable phases were identified with precipitates at the grain boundary and inside the matrix. They are richer in copper as the thickness decreases (increasing cooling rate). The structure size and the fine precipitates size, amount and distribution are responsible for the differences in hardness obtained.

3.3.2. Ductility

Owing to the difficulty in conducting reliable tensile tests on thin ribbons, a reversed bending test (180°) was used and the number of bending cycles to fracture, N_b, was taken as a measure of ribbon ductility. A bending test was previously used for ribbons to determine whether they were brittle or ductile [37]. The results in Fig. 13 indicate that N_b decreases with increasing copper content in the alloy and with increasing ribbon thickness. The first result is reasonable, because an increase in copper content reduces the ductility of Al–Cu alloys. The increase in ductility with reduction of ribbon thickness indicates that the structure (very fine structure and precipitates) obtained should be more ductile than the coarser structure. Plotting these results as a function of hardness and ribbon thickness in Fig. 14 indicates that the increase in hardness is accompanied by a decrease in ductility, N_b, as would be expected, and that the thinner ribbons acquire an increase in both hardness and ductility, i.e. that the fine precipitate and/or

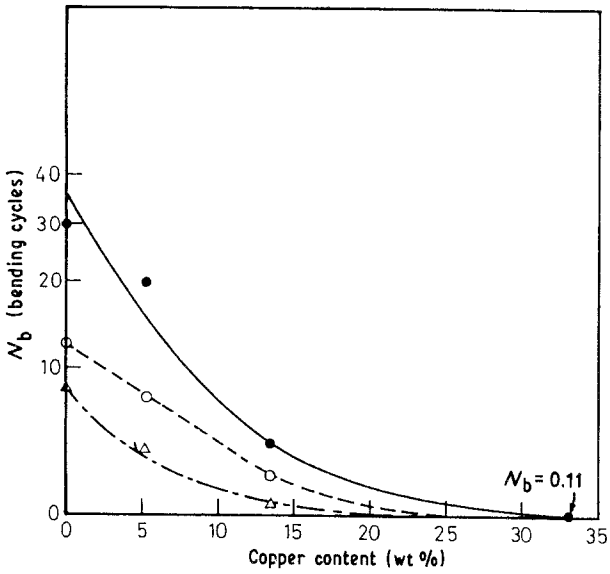

Figure 13 Influence of alloy copper content on the number of reversed bending cycles to fracture, N_b, for different ribbon average thicknesses, t: (——) 60 μm, (– – –) 120 μm, (— — —) 500 μm.

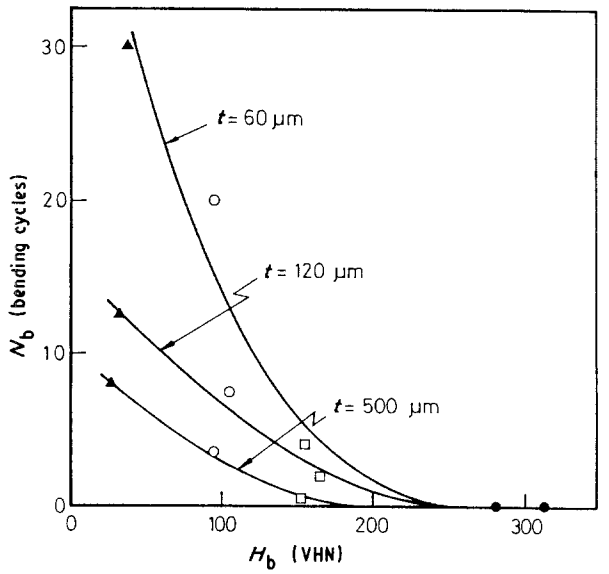

Figure 14 Influence of ribbon bulk Vicker's microhardness, H_b, and ribbon average thickness, t, on the number of reversed bending cycles to fracture, N_b. (▲) Pure Al (99.99%), (○) Al–5.23 wt % Cu, (□) Al–13.46 wt% Cu, (●) Al–33 wt % Cu.

metastable phase present in thin ribbons of 60 μm are not harmful but rather advantageous for the mechanical properties.

References

1. T. R. ANANTHARAM and C. SURYANARAYANA, "Rapidly Solidified Metals: A Technological Overview" (Trans Tech Publications, Switzerland, 1987) p. 47.
2. S. KAVESH, in "Metallic Glasses", edited by J. J. Gilman and H. J. Leamy (American Society for Metals, Metals Park, OH, 1978) pp. 36–73.
3. H. H. LIEBERMANN, *J. Crystal Growth* **70** (1984) 497.
4. J. R. BEDELL, Allied Chemical Corporation, US Pat. 3862658, 28 January 1975.
5. R. W. JECH, T. J. MOORE, T. K. GLASGOW and N. W. ORTH, *J. Metals* **36** (4) (1984) 41.
6. H. R. HILZINGER and S. HOCK, in "Metallic Glasses: Science and Technology", Vol. 1, edited by C. Hargitai, I. Bakonyi and T. Kemeny (Central Research Institute for Physics, Budapest, Hungary, 1981) p. 71.

7. L. A. DAVIES, N. DE CRISTOFARO and C. H. SMITH, *ibid.*, p 1.
8. H. H. LIEBERMANN, *Mater. Sci. Engng* **43** (1980) 203.
9. F. R. MOLLARD, in Proceedings of a symposium sponsored by the Solidification Committee of The Metallurgical Society of AIME at the TMS-AIME fall Meeting, Pittsburgh, Pennsylvania, 8 October 1980 (Metallurgical Society of AIME, 1980) pp. 1–16.
10. J-C. HUBERT, F. MOLLARD and B. LUX, *Z. Metallkde* **64** (1973) 835.
11. M. F. ABDEL-GHAFFAR, MSc thesis, Ain-Shams University, Cairo, Egypt (1985).
12. M. A. TAHA, N. A. EL-MAHALLAWY and M. F. ABDEL-GHAFFAR, *Mater. Sci. Engng* **A134** (1991) 1162.
13. M. A. TAHA, N. A. EL-MAHALLAWY, M. F. ABDEL-GHAFFAR and J. KLAAR, *ibid.* **A133** (1991) 758.
14. Å. ÖSTLUND and R. WEST, *Int. J. Rapid Solid.* **3** (1988) 177.
15. P. H. SHINGU and R. OZAKI, *Met. Trans.* **6A** (1975) 33.
16. H. A. DAVIES and B. G. LEWIS, *ibid.* **7A** (1976) 310.
17. N. A. EL-MAHALLAWY and M. A. TAHA, *J. Mater. Sci.* **6** (1987) 885.
18. M. COHEN, B. H. KEAR and R. MEHRABIAN, in "Proceedings of the 2nd International Conference on Rapid Solidification Processing", Reston, VA, USA, 23–26 March 1980 (Claitor's Baton Rouge, LA, 1980) pp. 1–23.
19. P. PREDECKI, A. W. MULLENDORE and N. J. GRANT, *Trans. Met. Soc. AIME* **233** (1965) 1581.
20. M. LEBO and N. J. GRANT, *Met. Trans.* **5** (1974) 1547.
21. J. P. DURAND, R. M. PELLOUX and N. J. GRANT, in "Rapidly Quenched Metals II", edited by N. J. Grant and B. C. Giessen (M.I.T. Press, Cambridge, Mass., 1976) p. 247.
22. K. K. SANKARAN and N. J. GRANT, *Mater. Sci. Engng* **44** (1980) 213.
23. M. A. MARCUS, *Acta. Metall.* **27** (1979) 893.
24. T. NAOHARA, A. INOUE, T. MASUMOTO and K. KUMADA, *Met. Trans.* **134** (1982) 337.
25. M. H. RAO, G. SRIDHAR and C. SURYANARAYANA, *Z. Metallkde* **74** (1983) 585.
26. M. H. RAO, G. SRIDHAR and C. SURYANARAYANA, *Int. J. Rapid Solid.* **1** (1985) 199.
27. C. E. MOBLEY, A. H. CLAUER and B. A. WILCOX, *J. Inst. Metals* **100** (1972) 142.
28. J. V. WOOD, *Mater. Design* **4** (1983) 673.
29. G. HAOUR, in Proceedings of a symposium, sponsored by the Solidification Committee of The Metallurgical Society of AIME at the TMS-AIME Fall Meeting, Pittsburgh, Pennsylvania, 8 October 1980 (Metallurgical Society of AIME, 1980) pp. 117–23.
30. M. LEBO and N. J. GRANT, *Met. Trans.* **5** (1974) 1547.
31. J-P. H-A. DURAND, R. M. FELLOUX and N. J. GRANT, *Mater. Sci. Engng* **23** (1976) 247.
32. KEN-ICHI MIYAZAWA and TAKAO CHOH, *J. Jpn Inst. Metals* **46** (1983) 717.
33. S. C. HUANG and H. C. FIEDLER, in Proceedings of a symposium sponsored by The Solidification Committee of The Metallurgical Society of AIME at The TMS-AIME Fall Meeting, Pittsburgh, Pennsylvania, 8 October 1980 (The Metallurgical Society of AIME, 1980) pp. 225–31.
34. S. C. HUANG, in "Rapidly Quenched Metals IV", edited by T. Masumoto and K. Suzuki (Japan Institute of Metals, Sendai, 1982) p. 35.
35. J. H. VINCENT, H. A. DAVIES and J. G. HERBETSON, *ibid.*, pp. 103–16.
36. L. KATGERMAN, H. KLEINJAN, R. W. E. KROPF and W. E. ZALM, in "Proceedings of the 2nd International Symposium on Materials and Energy from Refuse (MER 2)", Antwerp, Belgium, 20–22 October 1981.
37. A. RABINKIN, F. REIDINGER, J. MARTI and L. BENDERSKY, *Mater. Sci. Engng* **A133** (1991) 256.

Received 7 August
and accepted 27 November 1991